Mean-field Gaussian chain theory for semidilute theta chains in a slit

ARTICLE *in* THE JOURNAL OF CHEMICAL PHYSICS · DECEMBER 2001

Impact Factor: 2.95 · DOI: 10.1063/1.1420750

2 AUTHORS:

Iwao Teraoka
Polytechnic Institute of New York University
113 PUBLICATIONS **2,884** CITATIONS
SEE PROFILE

Peter Cifra
Slovak Academy of Sciences
96 PUBLICATIONS **1,025** CITATIONS
SEE PROFILE

Mean-field Gaussian chain theory for semidilute theta chains in a slit

Iwao Teraoka[a)]
Herman F. Mark Polymer Research Institute, Polytechnic University, Six MetroTech Center, Brooklyn, New York 11201

Peter Cifra
Polymer Institute, Slovak Academy of Sciences, Dúbravská Cesta 9, 842 36 Bratislava, Slovak Republic

(Received 24 April 2001; accepted 1 October 2001)

Mean-field Gaussian chain theory for nondilute polymer solutions is being applied to polymer chains in the theta condition confined to a slit in a wide range of concentrations. Various existing lattice chain theories were used to obtain the effective potential for the Gaussian chain. Calculation results for the monomer density profile, the partition coefficient, and the chain dimension across the slit at various concentrations were computed and compared with the results obtained in the lattice Monte Carlo simulations. The need for a higher concentration to flatten the density profile and to cause the weak-to-strong penetration transition, compared with athermal chains, was confirmed. At the monomer–monomer interaction widely used as the theta condition on the cubic lattice, the chain cluster theory by Freed and the random mixing approximation by Huggins provide a better agreement with the simulation results than the Flory model and the Guggenheim model do. The agreement is, however, not as good as the one for athermal chains. © *2001 American Institute of Physics.* [DOI: 10.1063/1.1420750]

I. INTRODUCTION

The density profile of polymer chains in confined space has been investigated extensively in Monte Carlo simulations.[1–12] The confining geometry was typically a slit between two impenetrable, nonadsorbing parallel walls. The profile is different between a weak confinement ($R_g \ll d$, where R_g is the radius of gyration of the isolated polymer chain in unconfined solution, and d is the slit width) and strong confinement ($R_g \gg d$). For weakly confined athermal chains, the density profile has a plateau in the middle but declines to extinction at the walls. The depletion layer at the wall has a thickness of $\sim R_g$.[13–15] As the concentration increases, monomers are driven toward the walls to avoid the strong repulsive interactions between chains, thinning the depletion layer. In the semidilute solution, the thickness of the depletion layer scales as ξ, the correlation length.[15,16] In the strong confinement, in contrast, the profile does not have a plateau at low concentrations, but with an increasing concentration and a concomitant decrease in ξ, the plateau appears.

Our recent simulation[7] revealed that, in the theta solvent, the appearance of the plateau in the strong confinement requires a much higher concentration than it does in the athermal solvent. This result mirrors another finding[7] that the partition coefficient is nearly unchanged from the dilute-solution value until the exterior concentration becomes several times as high as the overlap concentration. The flat partition coefficient is due to a missing driving force, a positive second virial coefficient.[8] With the third virial coefficient being the leading term in the interaction, the weak-to-strong penetration transition[15,16] in the partitioning requires a much higher concentration in the theta solvent compared with the athermal solvent. How the density profile and the partition coefficient change with concentration is sensitive to the interaction, especially at the theta condition where the repulsion by the excluded volume and the attractive monomer–monomer interaction compensate each other. The dependence may serve as a critical test of a thermodynamic theory for polymer chains in the unconfined solution.

Recently Teraoka and Wang developed a mean-field Gaussian chain theory for a nondilute solution of athermal chains confined to a slit.[17] The interaction between the polymer chains was incorporated into an effective potential field in which a chain with a Gaussian conformation grows. Since the monomer density trails off to zero at the slit walls, the interactions between the monomers diminish with a decreasing distance to one of the walls. So does the potential. The dependence of the potential field on the local monomer density was determined so that, when the same theory was applied to the unconfined solution, the chemical potential reproduces the existing semiempirical formula.[18,19]

The mean-field Gaussian chain theory allowed calculation of the monomer density across the slit, the chemical potential and the transverse dimension of the confined chain, and the partition coefficient at different concentrations. The results were in a good agreement with those obtained in lattice Monte Carlo simulations for self-avoiding walks in a wide range of concentrations.[17]

The thermodynamics of a confined solution in the theta condition has not been considered theoretically beyond the scaling theory.[20] The present contribution applies the formulation of the mean-field Gaussian chain theory and the results of lattice chain theories such as Flory's to the theta solution confined to a slit in a wide range of concentrations. Four

a)Author to whom correspondence should be addressed. Fax: 718-260-3125; electronic mail: teraoka@poly.edu

models of the lattice chain theory are compared. We present a method to calculate the monomer density profile, the partition coefficient, and the chain dimension across the slit. We will also compare the results of the calculation with those obtained in lattice Monte Carlo simulations. The comparison will tell which of the four models most closely describes the simulation results and what improvements are needed.

II. THETA CONDITION IN LATTICE CHAIN THEORIES

Our formulation relies on the expression of the free energy in bulk solutions to obtain the mean-field potential. We employ four models developed for lattice chains and capable of providing a formula for the free energy. Three of them express the free energy in a closed form. The Flory model[21] assumes random mixing of monomers with solvent molecules and neglects the segment connectivity. The latter was taken into account by Huggins.[22] The effect of nonrandom mixing was considered by Guggenheim.[23] The latter is called the quasichemical approximation.

In the lattice model with lattice coordinate Z, the sites are occupied by polymer chains consisting of N consecutive sites and solvent molecules, each occupying a single site. When two nonbonded monomers are next to each other on the lattice, we assign a negative contact energy $-\epsilon$. In the Flory model, the Helmholtz free energy A_{Fl} of the polymer solution is given as

$$\frac{A_{\mathrm{Fl}}}{n_{\mathrm{site}}k_BT}=\frac{\phi}{N}\ln\phi+(1-\phi)\ln(1-\phi)-(Z/2-1)\frac{\epsilon}{k_BT}\phi^2, \tag{1}$$

where n_{site} is the number of lattice sites in the system, k_BT is the thermal energy, and ϕ is the volume fraction. Here the bonded contacts were excluded from the interaction term. In the Huggins model, the free energy A_H is given as

$$\frac{A_H}{n_{\mathrm{site}}k_BT}=\frac{\phi}{N}\ln\phi+(1-\phi)\ln(1-\phi)-\frac{Z}{2}(1-\alpha\phi)\ln(1-\alpha\phi)-\frac{Z}{2}(1-\alpha)\frac{\epsilon}{k_BT}\phi q, \tag{2}$$

where $\alpha=2Z^{-1}(1-N^{-1})$ and $q=(1-\alpha)\phi/(1-\alpha\phi)$. In the Guggenheim model (first-order; follows the derivation by Nies[24]) the free energy A_G is given as

$$\frac{A_G}{n_{\mathrm{site}}k_BT}=\frac{\phi}{N}\ln\phi+(1-\phi)\ln(1-\phi)-\frac{Z}{2}(1-\alpha\phi)\ln(1-\alpha\phi)-\frac{Z}{2}(1-\alpha\phi)[2q\ln q+2(1-q)\ln(1-q)-2q\ln t-(1-2q)\ln(1-q-t)], \tag{3}$$

where t satisfies

$$\frac{\epsilon}{k_BT}=\ln\frac{(q-t)(1-q-t)}{t^2}. \tag{4}$$

A different approach to the lattice chain theory was proposed by Freed and co-workers.[25] In their lattice cluster theory, the free energy is expanded with respect to ϵ/k_BT and $1/Z$. Their explicit expression for the free energy A_{Fr} is given as

$$\frac{A_{\mathrm{Fr}}}{n_{\mathrm{site}}k_BT}=\frac{\phi}{N}\ln\phi+(1-\phi)\ln(1-\phi)-\frac{Z}{2}\frac{\epsilon}{k_BT}\phi^2+C_0(\phi)+C_1(\phi)\frac{\epsilon}{k_BT}+C_2(\phi)\left(\frac{\epsilon}{k_BT}\right)^2. \tag{5}$$

Three concentration-dependent functions C_0, C_1, and C_2 are given in Ref. 25.

We will use these expressions of the free energy for unconfined solutions in order to derive a potential function needed in our Gaussian chain theory for confined chains. The procedure will be explained in the next section.

The theta condition is determined from the vanishing second virial coefficient in the long-chain limit. For the cubic lattice ($Z=6$), the energy at the theta condition is given by $\epsilon/k_BT=1/(Z-2)=1/4$ in the Flory and Huggins models, and $\epsilon/k_BT=\ln(1+1/(Z-2))=\ln(5/4)\cong 0.2231$ in the Guggenheim model. In the Freed model, $\epsilon/k_BT\cong 0.2589$ gives the theta condition. In simulations, however, it was shown that $\epsilon/k_BT=0.2693$ gives the condition, as demonstrated in the phase diagram of polymer–solvent demixing, in the chain-dimension scaling, and in the second virial coefficient.[26] We also note here that none of these theoretical models provides the scaling exponent of 3 for the power relationship between the osmotic pressure and the concentration in the semidilute solution at the theta condition.

III. MEAN–FIELD GAUSSIAN CHAIN THEORY

Now we briefly review the mean-field theory for a Gaussian chain confined to a slit.[17] It is based on Casassa's original diffusion equation-based formulation for a single chain confinement[13,14] and de Gennes' refinement using Schrödinger equation.[15] The slit space extending in y and z directions is given by $0<x<d$, and the chain consists of N segments of length b. The Green function $G(\mathbf{r},\mathbf{r}';n)$ is equal to the probability density of finding the nth segment at $\mathbf{r}$ when the 0th segment is at $\mathbf{r}'$. We pay attention to the y, z-averaged Green function $G_x(x,x';n)$ defined as $G_x(x,x';n)\equiv\int dy\int dz G(\mathbf{r},\mathbf{r}';n)$. In a potential field $U(x)$, G_x satisfies

$$[\partial/\partial n-(b^2/6)\partial^2/\partial x^2+U(x)]G_x(x,x';n)=\delta(x-x')\delta(n). \tag{6}$$

We employ the mean-field potential $U(x)=N^{-1}f_m(\phi(x))$ for $0<x<d$, $U(x)=\infty$ otherwise. The potential at x is given as a function of the mean monomer density $\phi(x)$ that varies with x. Since the monomer density $\phi(x)$ is determined by the Green function, $G_x(x,x';n)$ needs to be obtained self-consistently.

The solution of Eq. (6) is formally given as

$$G_x(x,x';n)=\sum_{k=1}^{\infty}u_k(x)u_k(x')\exp(-n\epsilon_k), \tag{7}$$

where the kth eigenfunction $u_k(x)$ is expressed by a Fourier series,

$$u_k(x)=\sum_{j=1}^{\infty} a_{kj}u_{0j}(x) \quad (k=1,2,...), \tag{8}$$

with a_{kj} being the expansion coefficients and $u_{0j}(x)=(2/d)^{1/2}\sin(j\pi x/d)$ $(j=1,2,...)$. When $f_m=0$ (at $\phi=0$), $a_{kj}=\delta_{kj}$ with δ_{kj} being the Kronecker delta. Equation (6) is now represented in the matrix form,

$$\mathbf{M}\mathbf{a}_k=(N\epsilon_k)\mathbf{a}_k, \tag{9}$$

where $\mathbf{a}_k$ is the transpose of $[a_{k1},a_{k2},\ldots]$, and the elements of $\mathbf{M}$ are given as

$$M_{ij}=N\epsilon_{0i}\delta_{ij}+U_{ij} \quad (i,j=1,2,...), \tag{10}$$

where $N\epsilon_{0i}=N(b^2/6)(i\pi/d)^2=(i\pi R_g/d)^2$ with R_g being the radius of gyration of the unconfined chain, and

$$U_{ij}=\int_0^d u_{0i}(x)f(\phi(x))u_{0j}(x)dx. \tag{11}$$

Using a_{kj}, $\phi(x)$ is expressed as

$$\phi(x)\propto \sum_{j,m:\text{odd}} u_{0j}(x)u_{0m}(x)\sum_{k,l:\text{odd}} b_k b_l e_{kl}a_{kj}a_{lm}, \tag{12}$$

where

$$b_k=\sum_{j:\text{odd}} j^{-1}a_{kj}, \tag{13}$$

and

$$e_{kl}=\begin{cases}\dfrac{\exp(-N\epsilon_l)-\exp(-N\epsilon_k)}{N(\epsilon_k-\epsilon_l)} & (k\neq l)\\ \exp(-N\epsilon_k) & (k=l)\end{cases}. \tag{14}$$

We require that, when applied to the unconfined solution that has the monomer density $\phi(\mathbf{r})$ at $\mathbf{r}$, the solution of the following equation with $U(\mathbf{r})=N^{-1}f_m(\phi(\mathbf{r}))$ for every $\mathbf{r}$ in the system reproduce the thermodynamics known for the unconfined solution,

$$[\partial/\partial n-(b^2/6)\nabla^2+U(\mathbf{r})]G(\mathbf{r},\mathbf{r}';n)=\delta(\mathbf{r}-\mathbf{r}')\delta(n). \tag{15}$$

Two levels of approximation were employed for f_m. The first-order mean-field approximation assumes a uniform ϕ. It was shown that the potential function f_{m1} in the first-order approximation is the nonideal part of the chemical potential $\mu(\phi)$,

$$f_{m1}(\phi)=\mu(\phi)/k_BT-\ln\phi. \tag{16}$$

which is also called the excess chemical potential. In the lattice chain model, $\mu(\phi)$ refers to the change in the free energy when N consecutive unoccupied sites are replaced by a polymer chain. The reference for $\mu(\phi)$ is adjusted so that its nonideal part vanishes as $\phi\to 0$. In the lattice chain model, $\mu(\phi)$ is calculated from the free energy A by

$$\frac{\mu}{k_BT}=N\left(\frac{\partial}{\partial\phi}\frac{A}{n_{\text{site}}k_BT}\right)_{V,T}. \tag{17}$$

Using Eqs. (1)–(3) and (5), $f_{m1}(\phi)$ is calculated for each of the four models. In the Flory model,

$$\frac{f_{m1\text{Fl}}(\phi)}{N}=-\ln(1-\phi)-\frac{(Z-2)\epsilon}{k_BT}\phi. \tag{18}$$

In the Huggins model,

$$\frac{f_{m1,H}(\phi)}{N}=-\ln(1-\phi)+\frac{Z}{2}\alpha\ln(1-\alpha\phi)-\frac{Z}{2}\frac{\epsilon}{k_BT}\frac{q^2(2-\alpha\phi)}{\phi}. \tag{19}$$

In the Guggenheim model,

$$\frac{f_{m1,G}(\phi)}{N}=-\ln(1-\phi)+\frac{Z}{2}\alpha\ln(1-\alpha\phi)-\frac{Z}{2}\left(2(1-\alpha)\ln\frac{q(1-q-t)}{(1-q)t}-\alpha\ln\frac{(1-q)^2}{1-q-t}\right). \tag{20}$$

In the Freed model,

$$\frac{f_{m1,\text{Fr}}(\phi)}{N}=-\ln(1-\phi)-Z\frac{\epsilon}{k_BT}\phi+C_0'(\phi)+C_1'(\phi)\frac{\epsilon}{k_BT}+C_2'(\phi)\left(\frac{\epsilon}{k_BT}\right)^2, \tag{21}$$

where a constant was added to each f_{m1} to make it disappear in the dilute solution limit. In Eq. (21), the prime denotes the derivative. The self-consistency requires that Eqs. (9), (11), and (12), and one of the equations for f_{m1} [Eqs. (18)–(21)] be satisfied simultaneously.

We can improve the approximation of the mean-field potential by incorporating correlations in the local monomer density.[17] The procedure to evaluate this second-order mean-field potential $f_{m2}(\phi)$ is outlined in the Appendix. The correction by the second-order approximation was large and effective in bringing the calculation results in agreement with the simulation results for athermal chains.[17] It is, however, small in the theta solvent because of a near-zero first-order term in $f_{m1}(\phi)$ [see Eq. (A1)]. Below we will employ f_{m1} only.

The mean-field potential, especially $f_{m1}(\phi)$, will fail to provide an appropriate penalty against growing the Gaussian chain when the solution has a large fluctuation in the monomer density. The latter is the case at low concentrations. In dilute solutions, however, the potential is low, and therefore its effect on G_x is small. The shortcoming will be more obvious at around the overlap concentration ϕ^*. Fortunately in the theta solution, the potential is weak at around ϕ^*. We expect that our approach will decently describe the confined system, as long as we employ a correct expression of the free energy.

We prepared the plots of $f_{m1}(\phi)$ for the four models at their respective theta conditions for chains with the lengths used in the simulation ($N=100$, 1000, 2000). At $N=1000$ (not shown), the Flory model has the highest potential, and the Huggins model the lowest at all concentrations. The Freed model gives a relatively high potential at $\phi<0.2$, but the increase in f_{m1} slows down at higher concentrations.

We also prepared the plots of $f_{m1}(\phi)$ for the four models at $\epsilon/k_BT=0.2693$ that gives the theta condition in simula-

tion. At $N=1000$, the plot for the Freed model hovers around zero before it starts to deviate upward at around $\phi=0.09$. In the other models, especially in the Huggins and Guggenheim models, the curves hit deeply negative in a wide range of concentrations. The Flory model has a high potential at $\phi>0.2$, even in its poor solvent condition.

When f_{m1} is a decreasing function of ϕ at $\epsilon/k_BT=0.2693$, the overall chemical potential $\mu(\phi)$ given by Eq. (16) can also decrease in a certain range of ϕ. This prospect raises a concern of a two-phase solution; Our mean-field theory assumes a single phase. In the Freed model, $\mu(\phi)$ is always an increasing function even with $N=2000$. In the Huggins model with $N=1000$, $\mu(\phi)$ is a decreasing function in a wide range of ϕ, indicating a phase separation. With $N=100$, it is an increasing function. The plot of $\mu(\phi)$ is partly decreasing in the Flory and Guggenheim models for $N=1000$. Therefore we cannot use Flory, Huggins, or Guggenheim model in our mean-field Gaussian chain theory for $N=1000$ or 2000 at $\epsilon/k_BT=0.2693$. For $N=100$ at $\epsilon/k_BT=0.2693$, the Flory, Huggins, and Freed models can be used, but not the Guggenheim model.

In the theory for athermal chains, we allocated a different R_g at each concentration to account for the chain contraction at higher concentrations and a concomitant decrease in the confinement entropy.[17] Thus, the unperturbed eigenvalue $N\epsilon_{0i}$ in Eq. (10) decreased with an increasing concentration. This procedure is not necessary for the theta chains, because it was demonstrated that the chain dimension barely changes in unconfined solutions in a wide range concentrations.[8,27,28] Therefore we can safely use the same R_g and $N\epsilon_{0i}$ in semidilute solutions as those in the dilute solution limit. Toward the end of the discussion, we will examine this problem more carefully.

Another advantage of the theta solution is that R_g of the theta chains in the unconfined dilute solution can be used as it is to calculate $N\epsilon_{0i}$. Our simulations demonstrated that there is no need to employ another R_g for the Gaussian chain in order to produce the same density profile as that of the theta chain at low concentrations.[12] In athermal solutions, in contrast, the mean-field theory needs another R_g for the Gaussian chain so that it has the same confinement entropy as the one the athermal chain receives when it enters the slit.

The partition coefficient K is obtained as the ratio of the average monomer density $\phi_{\mathrm{AV}}=d^{-1}\int\phi(x)dx$ in the slit space to the density ϕ_E in the unconfined solution compared at the same chemical potential. In the first-order approximation,[17]

$$\ln\phi_{\mathrm{AV}}-\ln\left(\frac{8}{\pi^2}\sum_{k:\mathrm{odd}}\exp(-N\epsilon_k)b_k^2\right)=\ln\phi_E+f_{m1}(\phi_E). \tag{22}$$

Unlike the chains in unconfined semidilute solutions, those in confined semidilute solutions can change their dimensions when the monomers are forced to spread toward the slit walls. The mean-square end-to-end distance (x component) $\langle R_x^2\rangle$ of the confined Gaussian chain across the slit is calculated as

TABLE I. Polymer chains used in the simulations.

N	R_g	ϕ^*
100	5.34	0.207
1000	17.52	0.0635
2000	24.81	0.0452

$$\langle R_x^2\rangle=\int_0^d dx\int_0^d dx'(x-x')^2G_x(x,x';N)\Big/\int_0^d dx\int_0^d dx'G_x(x,x';N)$$
$$=\frac{d^2}{2}\left[\sum_{k:\mathrm{odd}}\exp(-N\epsilon_k)b_k[b_k-8\pi^{-2}g_k]-\sum_{k:\mathrm{even}}\exp(-N\epsilon_k)b_k'^2\right]\Big/\sum_{k:\mathrm{odd}}\exp(-N\epsilon_k)b_k^2, \tag{23}$$

where

$$g_k=\sum_j j^{-3}a_{kj},\quad b_k'=\sum_{j:\mathrm{even}}j^{-1}a_{kj}. \tag{24}$$

IV. SIMULATION METHOD

Cubic lattice Monte Carlo simulations were conducted for chains of $N=100$, 1000, and 2000 in a broad range of concentrations. The theta chains were generated by using $-\epsilon/k_BT=-0.2693$ for both intra- and intermolecular nonbonded contacts[26] as we noted earlier. The radius of gyration R_g in the dilute solution limit and the overlap concentration ϕ^*, defined as $(\phi^*/N)[2^{1/2}(R_g+0.204)]^3=1$,[7] are listed in Table I. The unit length is a lattice spacing.

The simulation procedure is similar to those employed in our preceding works.[7,8,11] A simple box of a slit space only was used for chains with $N=1000$ and 2000. A twin box consisting of a slit space and an unconfined space was used for chains with $N=100$. The simple box has a dimension of $L_x\times L_y\times L_z(L_y=L_z=100)$ with walls at $x=0$ and $x=1+L_x$. All sites in the box are available for occupancy by the monomers. The slit width d_{sim} is the distance between the walls and given as $d_{\mathrm{sim}}=1+L_x$. A periodic boundary condition was enforced in the y and z directions. Polymer chains were moved by reptation moves following the Metropolis rule.[29] In the twin box, the slit space and the unconfined space had a dimension of $L_x\times30\times50$ and $50\times30\times50$, respectively. A periodic boundary condition was applied in all directions except where there is a slit wall.

In the present contribution, we focus on the monomer density profile $\phi(x)$ and the chain dimension across the slit as well as the partition coefficient $K_{\mathrm{sim}}=\phi_{\mathrm{AV,sim}}/\phi_E$, where $\phi_{\mathrm{AV,sim}}$ is the average monomer density in the layers within the slit space. In the simple-box simulation, ϕ_E was taken to be the density at the center portion of the density profile when the profile had a plateau in the middle. In the twin-box simulation, ϕ_E is the average density in the unconfined space, and $\phi_{\mathrm{AV,sim}}$ is the average density in the slit space

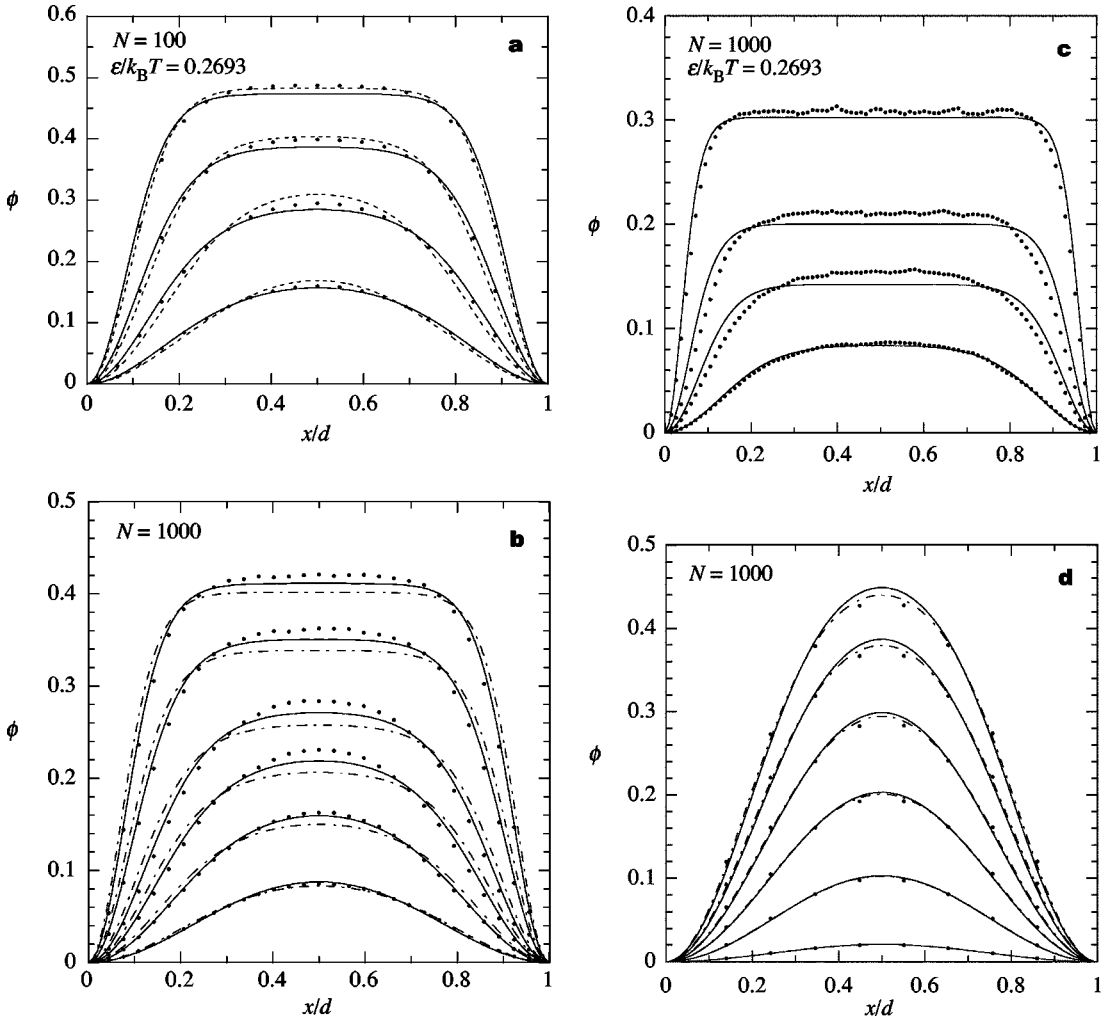

FIG. 1. Comparison of the monomer density profiles obtained in the simulation (dots) and those obtained in the present theory with the Huggins model at $\epsilon/k_BT=0.2693$ (dashed lines), the Freed model at $\epsilon/k_BT=0.2693$ (solid lines), and the Freed model at its own theta condition (dashed–dotted lines). (a) $N=100$, $d_{\mathrm{sim}}=20$. The average monomer density in the slit, $\phi_{\mathrm{AV,sim}}$, is 0.1, 0.2, 0.3, and 0.4 from bottom to top. (b) $N=1000$, $d_{\mathrm{sim}}=30$. $\phi_{\mathrm{AV,sim}}=0.0483$, 0.0966, 0.1448, 0.1931, 0.2759, and 0.3448 from bottom to top. (c) $N=1000$, $d_{\mathrm{sim}}=88$. $\phi_{\mathrm{AV,sim}}=0.0574$, 0.1149, 0.1724, and 0.2759 from bottom to top. (d) $N=1000$, $d_{\mathrm{sim}}=9$. $\phi_{\mathrm{AV,sim}}=0.0125$, 0.0625, 0.125, 0.1875. 0.25, and 0.3 from bottom to top.

excluding transition zones at the mouths of the slit. When a plateau was observed in the density profile within the slit space, the plateau density was equal to ϕ_E.

We note here that it is necessary to distinguish what is observed in simulations from what the theory calculates in the continuous space. First, it was demonstrated that the monomer density in the layers near the wall is extrapolated to zero on a hypothetical wall at a distance γ behind the physical wall on the lattice.[3,9,12] We called γ the penetration depth. For theta chains, $\gamma=0.36$ in dilute and semidilute solutions was established.[12] The theoretical wall-to-wall distance is $d=30.72$ when the slit has 29 layers available for monomer occupancy and hence $d_{\mathrm{sim}}=30$, for instance. Second, the average concentration $\phi_{\mathrm{AV,sim}}$ reported in the simulation is the average of densities sampled at the lattice points.[17] For comparison purpose only, the theory needs to calculate the average concentration at those values of x that correspond to the position of the layers in a given simulation box to compute K_{sim}. The latter average is different from ϕ_{AV}.

The theory allows calculation of the density profile of the chain ends. We did not collect the profile in the simulation, however.

V. RESULTS AND DISCUSSION

A. Density profile

To select the optimal thermodynamic model for the theta chains, we compare the monomer density profile between the theoretical results and the simulation results. Figures 1(a) and 1(b) show the results for chains with $N=100$ in a slit of $d_{\mathrm{sim}}=20$ ($d=20.72$) and for chains with $N=1000$ in a slit of $d_{\mathrm{sim}}=30$ ($d=30.72$), respectively. In part a, the curves obtained with the Freed model (solid lines) and the Huggins model (dashed lines) at $\epsilon/k_BT=0.2693$ are shown. The density profile is flatter at all concentrations in the Freed model than it is in the simulation. In contrast, the profile is more protrusive with the Huggins model at all concentrations except for $\phi_{\mathrm{AV,sim}}=0.4$ compared with the simulation. The Guggenheim model gives a negative slope in the chemical potential even for $N=100$, and therefore was not used for comparison. We also calculated the profiles for the four mod-

els in their respective theta conditions, but all of them gave flatter profiles than those obtained in the Freed model at $\epsilon/k_BT=0.2693$. The optimal $f_{m1}(\phi)$ for $N=100$ at $\epsilon/k_BT=0.2693$ appears to be the one between those given by the Freed and Huggins models at $\phi<0.4$. At higher concentrations, the optimal $f_{m1}(\phi)$ should be smaller than the one given by the Huggins model. In part b, we can compare only the Freed model with the simulation results, because all other models have a negative slope in the chemical potential for $N=1000$ at $\epsilon/k_BT=0.2693$. The difference between the theoretical curves and simulation results is similar to the one we saw in part a, except for the lowest concentration. The theoretical curves obtained for the model's theta condition are much flatter than those at $\epsilon/k_BT=0.2693$, because the interaction is too strong when ϵ/k_BT is smaller.

It is now apparent that the theoretical curves with the four models at their respective theta conditions do not provide a good agreement with the simulation results. At $\epsilon/k_BT=0.2693$, the Freed model has an edge because the system does not phase-separate even for $N=2000$ and the agreement with the simulation results is reasonable. The Huggins model can also be used for short-chain systems that do not phase-separate. The agreement with the simulation results is as good as that of the Freed model.

The profiles of chains with $N=1000$ in a weak confinement ($R_{g0}/d=0.199$) and a strong confinement ($R_{g0}/d=1.947$) are shown in Figs. 1(c) and 1(d), respectively. The solid lines are the results with the Freed model at $\epsilon/k_BT=0.2693$. The discrepancy between the simulation results and the theory in the weak confinement is similar to the one shown in Figs. 1(a) and 1(b). In the strong confinement, however, the theoretical curves are more protrusive at the slit center than the simulation profiles are. The latter comparison indicates that the interaction is stronger in the strong confinement than it is in the bulk solution and in the weak confinement. Here we see a limit of our approximation. It is necessary to have an expression of the interaction that takes into account the two-dimensional nature of the confined chains. The root mean square end-to-end distance of the chains in the slit of $d=9$ is around 47 at $\phi_{\mathrm{AV,sim}}=0.0125$, much greater than d. Interestingly, the agreement between the theoretical curves and the simulation results is better with the Freed model at its own theta condition. It is, however, a coincidence.

B. Partition coefficient

We now look at the weak-to-strong penetration transition. Figure 2(a) shows how the partition coefficient K increases with concentration ϕ_E in the unconfined solution equilibrated with the slit space for the chains in different slit widths. The number adjacent to each curve indicates R_g/d. The Freed model with $N=1000$ at $\epsilon/k_BT=0.2693$ was employed in the calculation. The partition coefficient first decreases with an increasing ϕ_E before it turns to increase sharply (weak-to-strong penetration transition). The decrease is due to a negative $f_{m1}(\phi)$ at $\phi<0.09$. The sharp upturn is more striking compared with the one we observed in the partitioning of the athermal chains.[7,17] At the theta condition of the Freed model, however, there is no decrease in K, as shown in Fig. 2(b). The slope of the tangent to each curve at $\phi=0$ is zero, because of a missing linear term in $f_{m1}(\phi)$, but quickly turns positive. The increase in K occurs at a higher concentration in both (a) and (b) compared with athermal chains because of a weaker $f_{m1}(\phi)$.

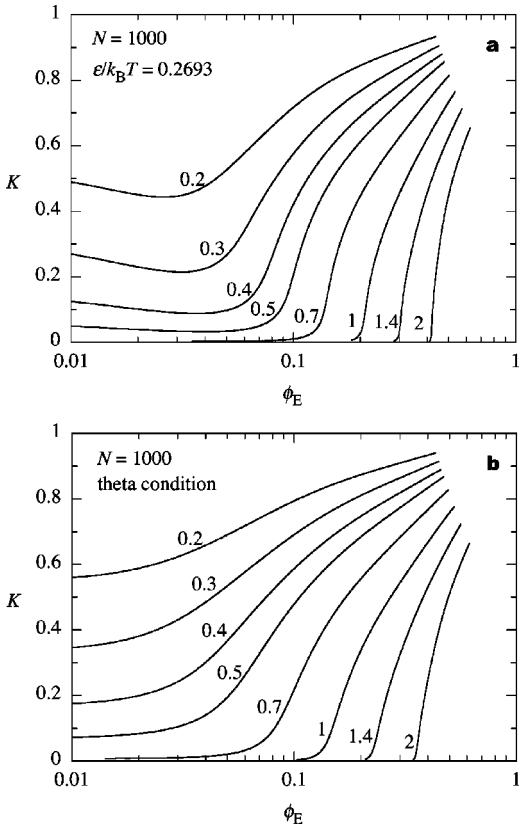

FIG. 2. Partition coefficient K obtained with the Freed model for $N=1000$ in various slit widths is plotted as a function of the exterior concentration ϕ_E. The relative chain dimension R_{g0}/d is indicated adjacent to each curve. (a) $\epsilon/k_BT=0.2693$, (b) theta condition of the model.

Figure 3 compares the partition coefficient between theory and simulation for chains with $N=1000$ in a slit of $d_{\mathrm{sim}}=30$. All of the theoretical curves (dashed lines) obtained in the respective theta conditions, except for the Hug-

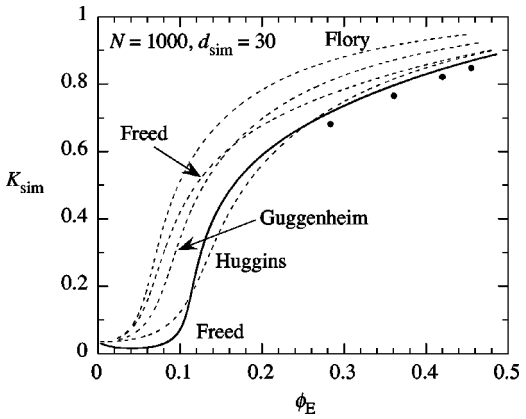

FIG. 3. Partition coefficient K_{sim} obtained in the simulation for chains with $N=1000$ in the slit of $d_{\mathrm{sim}}=30$, plotted in circles as a function of ϕ_E. The solid line was obtained with the Freed model at $\epsilon/k_BT=0.2693$. The dashed lines were obtained with the four models in their respective theta conditions.

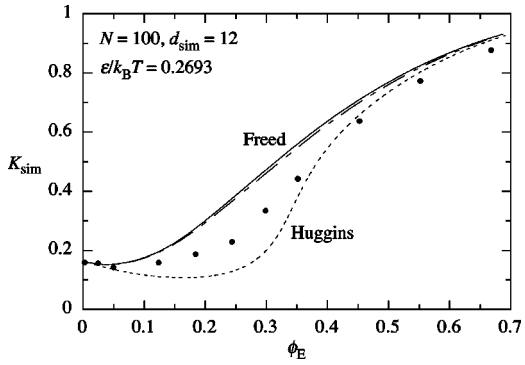

FIG. 4. Partition coefficient $K_{\rm sim}$ obtained in the simulation for chains with $N=100$ in the slit of $d_{\rm sim}=12$, plotted in circles as a function of ϕ_E. The solid and dashed lines were obtained with the Freed and Huggins models, respectively, at $\epsilon/k_BT=0.2693$. The dashed–dotted line was obtained using the Freed model with the chain swelling taken into account.

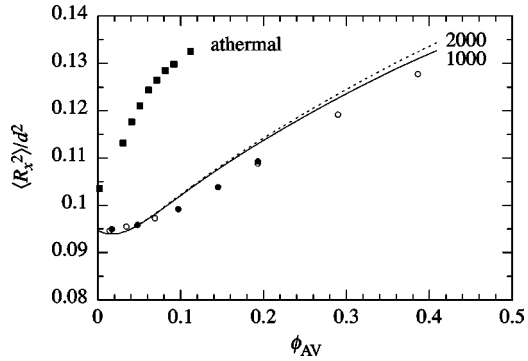

FIG. 5. The mean square of the x-component in the end-to-end vector for chains confined to a slit, $\langle R_x^2\rangle$, reduced by d^2. Symbols are for simulation data; $N=1000$, $d_{\rm sim}=30$ (closed circles) and $N=2000$, $d_{\rm sim}=30$ (open circles). Dashed and solid lines were obtained with the Freed model at $\epsilon/k_BT=0.2693$ for $N=1000$ and 2000, respectively. Simulation data obtained for athermal chains with $N=2000$, $d_{\rm sim}=31$ are shown as the closed squares for reference.

gins model, are located higher than the curve (solid line) obtained with the Freed model at $\epsilon/k_BT=0.2693$ which is slightly higher than the simulation results. The initial dip in $K_{\rm sim}$ of the latter is due to a negative f_{m1}. The mismatch between theory and simulation is more obvious for chains with $N=100$ in a slit of $d_{\rm sim}=12$, shown in Fig. 4. Calculation results were obtained with the Freed and Huggins models at $\epsilon/k_BT=0.2693$. At $\phi<0.4$, the simulation results are between those of the two models. At higher concentrations, both models give a greater $K_{\rm sim}$.

It is interesting to see a small dip in $K_{\rm sim}$ of the simulation data at $0<\phi<0.1$ before it increases at higher concentrations. We can ascribe the dip to the clustering of weakly associating chains.[7] Clustering increases the apparent chain size, thereby making the partitioning into the slit more difficult. The dip may, however, suggest that, at $\epsilon/k_BT=0.2693$, either the unconfined solution has a negative second virial coefficient or the confined solution has a positive second virial coefficient while the unconfined solution is still at theta. Further studies are needed.

How the partition coefficient depends on ϕ_E is extremely sensitive to the interaction between solutes. The high sensitivity is manifested in Fig. 4 as the difference in the theoretical plot for $K_{\rm sim}$ between the two models. From the comparison between theory and simulations, we can say that the Freed model overestimates the interaction at all concentrations and the Huggins model underestimates it at low concentrations, but overestimates at high concentrations.

C. Chain dimension across the slit

Figure 5 compares the chain dimension $\langle R_x^2\rangle$ in the direction perpendicular to the slit walls. Simulation results were obtained with the Freed model for chains of $N=1000$ and 2000 in a slit of $d_{\rm sim}=30$. The chain swells with an increasing concentration in the direction perpendicular to the slit walls, as monomers are forced to spread toward the walls. The results for two different chain lengths are overlapped, because in this strong confinement the fundamental mode $[u_{01}(x)]$ dominates for the two chain lengths. The theory with the Freed model well describes the swelling, although it overestimates the swelling slightly at most concentrations. Figure 5 also shows the result for athermal chains of $N=2000$ in a slit of $d_{\rm sim}=31$. Compared with the athermal chains strongly confined to the slit, the increase in $\langle R_x^2\rangle$ of the theta chains requires a much higher $\phi_{\rm AV}$. The driving force to spread the monomers toward the walls is much weaker in the theta condition.

D. Effect of chain swelling in the theta condition

Previous computer simulation results[8,27,28] show that the chain dimension in the unconfined solution maximizes at around the overlap concentration. Although the change is smaller than it is in the athermal chains, it may affect the partitioning that is sensitive to the interactions. We use here the following empirical formula,

$$R/R_0=0.3391\phi-0.7501\phi^2+0.3754\phi^3, \tag{25}$$

where R is the root-mean-square end-to-end distance, and R_0 is its value in the dilute solution limit. Simulation data[8] for $N=100$ in the range of $0<\phi<0.7$ were used for the fitting. At its maximum, $R/R_0\cong 1.044$. With $R_g/R\cong 6^{-1/2}$, we can evaluate the unperturbed eigenvalues $N\epsilon_{0i}$ at each concentration of the confined solution. The rest of the calculation is unchanged. The result is shown by a dashed–dotted line in Fig. 4. The effect of the chain swelling is minuscule and is not sufficient to explain the dip in K at low concentrations. We also compared the density profiles, but the difference was too small to effectively display it in the figure.

E. Sensitivity to the contact energy

The density profile of confined chains exhibits a different pattern, depending on ϵ/k_BT, as shown in Fig. 6. Compared at $\phi_{\rm AV,sim}=0.049\,82$ for chains with $N=1000$, athermal chains have the most widely spread profile, despite the strongest confinement. Note that the radius of gyration in the dilute solution limit is the greatest in athermal chains. With an increasing attraction between monomers, the profile becomes more centered in the middle of the slit. In the low concentration limit, the order would be reversed.

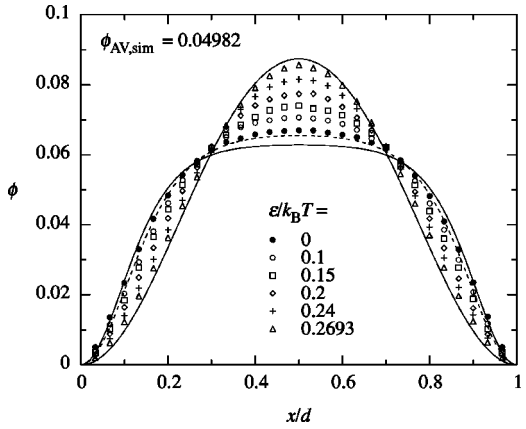

FIG. 6. Sensitivity of the density profile to the contact energy. Symbols were obtained in simulations for chains with $N=1000$ in a slit of $d_{sim}=30$ with the values of ϵ/k_BT indicated in the legend. Solid lines were obtained with the Freed model for $\epsilon/k_BT=0.2693$ and 0. The dashed line was obtained in the second-order mean-field approximation with the Ohta–Oono formula for the osmotic pressure.

We calculated the theoretical profiles using the Freed model for $\epsilon/k_BT=0$ and 0.2693, which are displayed as solid lines. The theoretical profile at the center of the slit is higher than the simulation profile at $\epsilon/k_BT=0.2693$, but lower at $\epsilon/k_BT=0$. The potential function of the Freed model for $\epsilon/k_BT=0$ is too strong. For the athermal chains, another profile was calculated in the same way as done before[17] by using the Ohta–Oono formula for the osmotic pressure.[18,19] The second-order mean-field approximation was employed. The agreement with the simulation results is much better compared with the one obtained in the lattice chain theories. The data for the radius of gyration and the partition coefficient in the low concentration limit are not available for the other values of ϵ/k_BT, and therefore we could not obtain theoretical results. With these data, the mean-field Gaussian chain theory would be able to predict the density profile in the slit and the partition coefficient at higher concentrations.

VI. CONCLUDING REMARKS

We have shown that the density profile and the partition coefficient reflect sensitively the interaction between polymer chains. The concentration dependences of the profile and the partition coefficient agree with the theory if the chemical potential is between those given by the Freed model and the Huggins model at the same contact energy as the one used in the simulation. We expect the higher-order terms yet to be determined in the perturbation expansion of the Freed model will account for the discrepancy. The comparison raises a hope that we might be able to find the optimal expression for $f_m(\phi)$. Further studies are needed.

The existing discrepancy in the contact energy between theory and simulation for unconfined chains in the theta condition needs to be resolved also. We note here that the low potential f_{m1} as seen in the Freed model at $\epsilon/k_BT=0.2693$ over an extended concentration range may lead to an error in the estimate of the theta condition in the simulation.

ACKNOWLEDGMENTS

The authors acknowledge support from the NSF DMR-9876360. P.C. acknowledges partial support by the Grant Agency for Science (VEGA), Grants Nos. 2/7056/21 and 2/7076/21. The use of computer resources of the Computing Center of SAS is gratefully acknowledged.

APPENDIX

In the mean-field Gaussian chain theory for confined athermal chains, the second-order mean-field approximation was also employed to account for the effect of the local monomer density fluctuations.[17] The potential function $f_{m2}(\phi)$ was expressed as

$$f_{m2}(\phi)=f_{m1}(\phi)+\ln[\cosh(f'_{m1}(\phi)\times\langle\Delta\phi(\mathbf{r}_1)\Delta\phi(\mathbf{r}_2)\rangle^{1/2})], \tag{A1}$$

where the monomer density correlation $\langle\Delta\phi(\mathbf{r}_1)\Delta\phi(\mathbf{r}_2)\rangle$ was taken with respect to two points $\mathbf{r}_1$ and $\mathbf{r}_2$ along a polymer chain. It was shown that

$$\langle\Delta\phi(\mathbf{r}_1)\Delta\phi(\mathbf{r}_2)\rangle=\frac{3}{2}\left(\frac{2}{\pi}\right)^{3/2}\frac{\phi^*\phi}{P+\phi P'}\left(\frac{\xi}{R_g}\right)^{-2}\left[1-(1+\xi^2/R_g^2)^{3/2}+\frac{3}{2}\xi/R_g+(\xi/R_g)^3\right], \tag{A2}$$

where ϕ^* is the overlap concentration, P is the osmotic compressibility, and ξ is the correlation length. For the latter, we use a formula that we obtained from the results of light scattering experiment for theta solutions by Brown and Nicolai,[30]

$$\xi/R_{g0}=(1+0.636\phi/\phi^*)^{-1}/\sqrt{3}. \tag{A3}$$

The compressibility is different from model to model. In the Huggins model, for instance, P is given as

$$P(\phi)=1-N\left[1+\phi^{-1}\ln(1-\phi)-\frac{Z}{2}(\alpha+\phi^{-1}\ln(1-\alpha\phi))+\frac{Z\epsilon}{k_BT}\frac{(1-\alpha)^2}{\alpha}\left(\frac{1}{1-\alpha\phi}+\frac{1}{\alpha\phi}\ln(1-\alpha\phi)\right)\right]. \tag{A4}$$

[1] M. R. L. Abadie and J. Dayantis, Macromol. Theory Simul. **5**, 93 (1996).
[2] Y. Wang and I. Teraoka, Macromolecules **30**, 8473 (1997).
[3] A. Milchev and K. Binder, Eur. Phys. J. B **3**, 477 (1998); **13**, 607 (2000).
[4] P. Cifra and T. Bleha, Macromol. Theory Simul. **8**, 603 (1999).
[5] Y. Wang and I. Teraoka, Macromolecules **33**, 3478 (2000).
[6] I. Teraoka and Y. Wang, Macromolecules **33**, 6901 (2000).
[7] P. Cifra, T. Bleha, Y. Wang, and I. Teraoka, J. Chem. Phys. **113**, 8313 (2000).
[8] P. Cifra and T. Bleha, Macromol. Theory Simul. **9**, 555 (2000).
[9] J. De Joannis, J. Jimenez, R. Rajagopalan, and I. Bitsanis, Europhys. Lett. **51**, 41 (2000).
[10] Y. Wang, I. Teraoka, and P. Cifra, Macromolecules **34**, 127 (2001).
[11] P. Cifra and T. Bleha, Macromolecules **34**, 605 (2001).
[12] I. Teraoka, P. Cifra, and Y. Wang, Macromolecules **34**, 7121 (2001).
[13] E. F. Casassa, J. Polym. Sci., Polym. Lett. Ed. **5**, 773 (1967).
[14] E. F. Casassa and Y. Tagami, Macromolecules **2**, 14 (1969).

[15] P. G. de Gennes, *Scaling Concepts in Polymer Physics* (Cornell University Press, Ithaca, 1979).
[16] M. Daoud and P. G. de Gennes, J. Phys. (Paris) **38**, 85 (1977).
[17] I. Teraoka and Y. Wang, J. Chem. Phys. **115**, 1105 (2001).
[18] T. Ohta and Y. Oono, Phys. Lett. **89A**, 460 (1982).
[19] Y. Oono, Adv. Chem. Phys. **61**, 301 (1985).
[20] E. Raphael and P. Pincus, J. Phys. II **2**, 1341 (1992).
[21] P. J. Flory, J. Chem. Phys. **10**, 51 (1942).
[22] M. L. Huggins, Ann. N.Y. Acad. Sci. **43**, 1 (1942).
[23] E. A. Guggenheim, *Mixtures* (Oxford University Press, London, 1952).
[24] E. Nies and P. Cifra, Macromolecules **27**, 6033 (1994).
[25] D. Buta, K. Freed, and I. Szleifer, J. Chem. Phys. **112**, 6040 (2000).
[26] A. Z. Panagiotopoulos, V. Wong, and M. A. Floriano, Macromolecules **31**, 912 (1998).
[27] O. F. Olaj, T. Petrik, and G. Zifferer, Macromol. Theory Simul. **6**, 1277 (1997).
[28] O. F. Olaj, T. Petrik, and G. Zifferer, J. Chem. Phys. **107**, 10214 (1997).
[29] N. Metropolis, A. W. Rosenbluth, M. N. Rosenbluth, A. H. Teller, and E. Teller, J. Chem. Phys. **21**, 1087 (1953).
[30] W. Brown and T. Nicolai, Colloid Polym. Sci. **268**, 977 (1990).